Journal of Hazardous Materials 241–242 (2012) 418–426

Contents lists available at SciVerse ScienceDirect

Journal of Hazardous Materials

journal homepage: www.elsevier.com/locate/jhazmat

Utilization of waste phosphogypsum to prepare hydroxyapatite nanoparticles and its application towards removal of fluoride from aqueous solution

Deyi Zhang[a,b,*], Heming Luo[a], Liwen Zheng[a], Kunjie Wang[a], Hongxia Li[a], Yi Wang[a], Huixia Feng[a]

[a] College of Petrochemical Technology, Lanzhou University of Technology, Lanzhou 730050, China
[b] State Key Laboratory of Gansu Advanced Non-ferrous Metal Materials, Lanzhou University of Technology, Lanzhou 730050, China

HIGHLIGHTS

- A novel approach on recycle of waste phosphogypsum was exploited.
- Phosphogypsum was utilized to prepare hydroxyapatite nanoparticles with high purity.
- nHAp derived from PG exhibits excellent adsoprtion capacity for fluoride.
- Fluoride adsorbs onto nHAp mainly by electrostatic interaction and hydrogen bond.

GRAPHICAL ABSTRACT

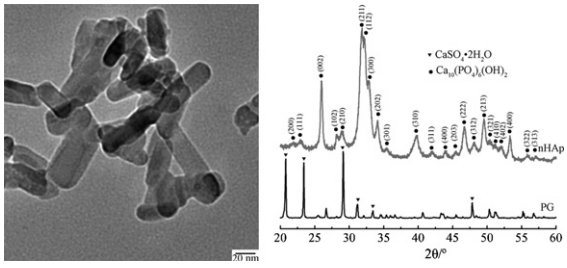

ARTICLE INFO

Article history:
Received 24 May 2012
Received in revised form 3 September 2012
Accepted 27 September 2012
Available online 6 October 2012

Keywords:
Phosphogypsum
Hydroxyapatite nanoparticles
Adsorption
Fluoride

ABSTRACT

In the present study, waste phosphogypsum (PG) was utilized firstly to prepare hydroxyapatite nanoparticles (nHAp) via microwave irradiation technology. The nHAp derived from PG exhibited a hexagonal structure with the particle size about 20 nm × 60 nm and high purity. Meanwhile, the adsorption behaviour of fluoride onto the nHAp derived from PG was investigated to evaluate the potential application of this material for the treatment of the wastewater polluted with fluoride. The results indicate that the nHAp derived from PG can be used as an efficient adsorbent for the removal of fluoride from aqueous solution. The maximum adsorption capacities calculated from Langmuir–Freundlich model were 19.742, 26.108, 36.914 and 40.818 mg F^-/g nHAp for 298, 308, 318 and 328 K, respectively. The pseudo-second order kinetic model was found to provide the best correlation of the used experimental data compared to the pseudo-first order and the adsorption isotherm could be well defined by Langmuir–Freundlich equation. The adsorption mechanism investigation shows that electrostatic interaction and hydrogen bond are the main driving force for fluoride uptake onto nHAp derived from waste PG.

1. Introduction

Phosphogypsum (PG) is a waste by-product generated during the wet process manufacture of phosphorus fertilizer, which is mainly composed of gypsum ($CaSO_4{\cdot}2H_2O$) but also contains some impurities of environmental concern, such as P_2O_5, fluorides and metal elements (e.g., Fe, Mn, Al, Mg, etc.) [1,2]. Worldwide PG production is very large, it is estimated that more than 100–280 Mton PG is produced annually [3,4]. In present, only 15% of world PG production is recycled as building materials, agricultural fertilizers or soil stabilization amendments and as set controller in the manufacture of Portland cement [5–7]. The remaining 85% is stored into piles near the factory, occupying considerable land areas and causing serious environmental damage [1,8]. Therefore, recycling and minimizing the negative effects of this waste increasingly arouses the attention of researchers all around the world.

Hydroxyapatite (HAp), with nominal composition $Ca_{10}(PO_4)_6(OH)_2$, has gained its prominence due to its biocompatibility and osteoconductivity since it is the essentially hard, analogical composition of human bone mineral. As such, HAp

* Corresponding author at: College of Petrochemical Technology, Lanzhou University of Technology, Lanzhou 730050, China. Tel.: +86 13919114108; fax: +86 9312756296.
E-mail addresses: xixizhang@lut.cn, lzdeyizhang@yahoo.cn (D. Zhang).

0304-3894/$ – see front matter © 2012 Elsevier B.V. All rights reserved.
http://dx.doi.org/10.1016/j.jhazmat.2012.09.066

Table 1
Chemical composition of PG and nHAp derived from PG (wt.%).

Oxides	K_2O	MgO	Al_2O_3	Fe_2O_3	MnO_2	SiO_2	SO_3	CaO	P_2O_5
PG	1.47	0.07	1.04	0.95	0.46	5.55	37.44	46.10	6.92
nHAp	0.66	0.03	0.21	0.00	0.00	0.00	0.72	55.83	42.56

has been widely used as a bone substitute and ceramic implants [9–11]. In addition, HAp can be extensively used in biomedicine, catalyst or catalyst support, biosensor and sewage treatment [10–14]. Moreover, HAp has also been recognized for its potential in trapping and retention of toxic heavy metals and anion in ground water and soil [14–18]. For example, the application of HAp in the treatment of fluoride containing water has shown an excellent capability for the uptake of F^- ion [16]. Depending on the application, there is often a need for the nanoparticles to be in a particular size range. Various techniques have been employed to prepare nanosized hydroxyapatite particles (nHAp), such as coprecipitation method [19], sol–gel procedures [20], hydrothermal preparation [21] and microwave synthesis routes [22,23]. The microwave synthesis of nanosized HAp offers several advantages over other techniques including fast reaction, rapid heating, narrow particle distribution, high yield and excellent thermal stability, which contribute to it being one of the most effective processing methods for nanomaterials [23,24].

In this work, we proposed a new approach to recycle the phosphogypsum waste. PG was utilized firstly as raw material to prepare nHAp via microwave irradiation technology. The adsorption behaviour of the nHAp derived from PG for fluoride was also investigated to evaluate the potential application of this material in the treatment of the wastewater polluted with fluoride.

2. Experimental

2.1. Raw materials

The phosphogypsum waste samples used in this study were collected from the phosphorus fertilizer factory of Wengfu Group Co., Ltd. in Gansu, China. The chemical composition of the PG was evaluated by using energy dispersive X-ray spectroscopy (EDS) and the results were presented in Table 1.

2.2. Preparation of nHAp

The flowchart of preparing nHAp particles from waste phosphogypsum via microwave irradiation is shown in Fig. 1. In detail, 2 g of phosphogypsum was added into 50 mL of hydrochloric acid solution (10%), the mixture was then vigorously stirred for about 24 h and then filtrated through 0.45 μm membrane filter. After which, enough sodium hydroxide solution (8%) was added to adjust the pH of the filtrate to 9, and the solution was filtered again. And then, 20 mL of diammonium phosphate solution (26%) was slowly dropped into the filtrate under vigorous stirring. Immediately after, the pH of the mixed solution was adjusted to about 11 with sodium hydroxide solution (8%) to get a translucent colloid. The colloid was then moved to a 3-mouth flask and placed in a microwave reactor of 500 W powers with a refluxing and stirring system. The reaction was performed at 60 °C for 4 h. After cooling to room temperature, the precipitate was separated from the solution using a 0.45 μm membrane filter and washed with deionized water and ethanol. The washed precipitate was dried at 120 °C for 4 h under vacuum conditions, and ground into fine powder. The powder was then calcined at 500 °C for 2 h and cooled to ambient temperature to get nHAp particles.

2.3. Materials characterizations

The chemical composition of the PG and nHAp derived from PG was evaluated by using energy dispersive X-ray spectroscopy (EDS, JSM-5600LV, JEOL Ltd., Japan), Powder X-ray diffraction (XRD) patterns recorded by a PANalytica X'Pert Pro diffractometer were performed to identify the phase compositions of PG and nHAp. The particle size and morphology of the nHAp particles were characterized by transmission electron microscopy (TEM, JEM-2010, JEOL Ltd., Japan).

2.4. Adsorption and analytical methods

Adsorption experiments were performed in a shaking thermostatic gas bath at 298, 308, 318 and 328 K for a period of 24 h at 160 rpm using 100 mL polytetrafluor ethylene (PTFE) Erlenmeyer flasks with rubber plug. A stock solution of fluoride (1 g F^-/L) was prepared by dissolving the required amount of NaF in distilled water. The stock solution was diluted with distilled water to give the appropriate concentration of the working solutions. Batch adsorption experiments were conducted by contacting 0.1 g of nHAp samples with 100 mL of fluoride solution of desired concentration, temperature and pH. After continuous shaking, the solid was separated using a 0.45 μm membrane filter and the concentration of F^- was measured using a fluoride ion selective electrode (PHS-25) (Shanghai Precision&Scientific Instrument Co. Ltd., China). Effect of pH was investigated in the initial pH range of 2–11 at 298 K with adsorbent dose of 1 g/L at 100 mg F^-/L of fluoride concentration. Different dose of nHAp (1–10 g/L) was applied to evaluate the percent removal of fluoride from 10 to 50 mg F^-/L solution at neutral pH. The mixtures were shaken (24 h) at 298k until equilibrium was reached. The adsorption kinetics studies were

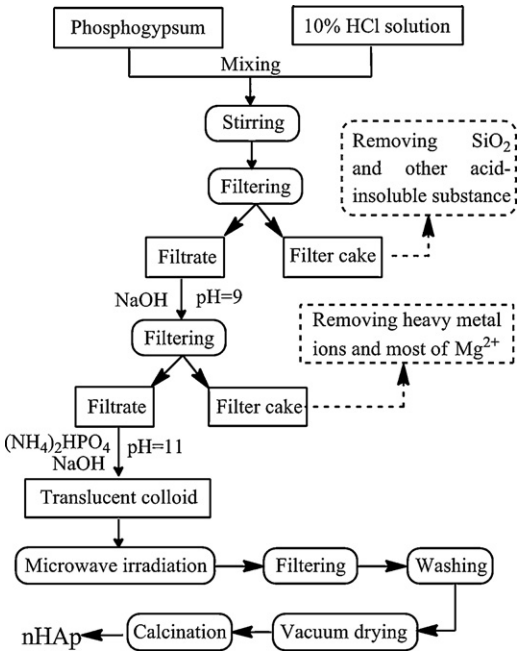

Fig. 1. Flowchart of preparing nHAp particles from PG.

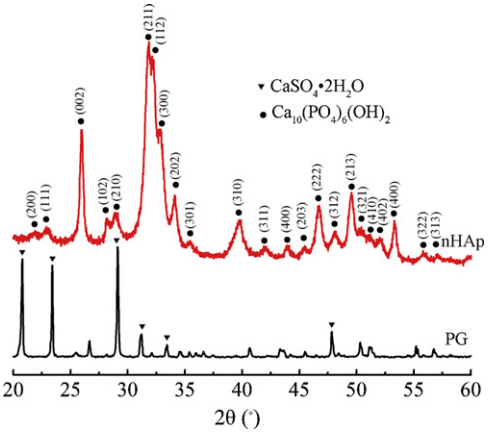

Fig. 2. XRD patterns of the raw PG and nHAp derived from PG.

conducted at 298, 308, 318 and 328 K for 24 h with an adsorbent dose of 1 g/L using 100 mL 20 mg F^-/L initial solution.

The adsorption capacity of fluoride (mg F^-/g) onto the nHAp was calculated according to:

$$q_e = \frac{(c_0 - c_e)V}{W} \quad (1)$$

where q_e (mg F^-/g) is the amount of fluoride adsorbed per unit mass of nHAp, c_0 and c_e are the initial and equilibrium concentrations (mg F^-/L) of fluoride in solution, respectively; V is the solution volume (L); and W is the weight (g) of nHAp.

The percent removal of fluoride from aqueous solution was calculated by the following equation:

$$\%\text{Removal} = \frac{c_0 - c_e}{c_0} \times 100 \quad (2)$$

Adsorption experiments were performed in triplicate, and the results are the averages of the three experiments.

2.5. Desorption experiments

Desorption studies were carried out by using the fluoride-adsorbed nHAp. First the fluoride-adsorbed nHAp was generated by adsorbing 50 mg F^-/L fluoride solution on 10 g/L nHAp at neutral pH. After the equilibration, the residue was filtered and the filtrate was measured for fluoride content. The fluoride-adsorbed nHAp samples were air dried for 24 h and then dispensed in 100 mL of 0.001 N HCl, 0.001 N NaOH, and neutral distilled water, respectively. The solutions were then shaken for about 24 h at 298 K after which the fluoride amount desorbed into the solution was determined as described in Section 2.4.

3. Results and discussion

3.1. Characterization of nHAp

Fig. 2 shows the XRD patterns of the raw PG and nHAp particles derived from PG. As shown in Fig. 2, the XRD pattern of the raw PG sample shows some main peaks at diffraction angles of 20.72°, 23.37°, 29.11°, 31.13°, 33.34° and 43.83°. The peaks are strong and characterized by gypsum ($CaSO_4 \cdot 2H_2O$) as the main phase composition of the PG wastes (re. PDF#33-0311). The other weak peaks are attributed to the presence of minor phases, such as silicate, phosphate and metallic oxide impurities, e.g. Fe, Mn, Al and Mg. All the diffraction peaks displayed in the XRD pattern of the nHAp derived from PG were easily indexed to pure hexagonal structural HAp (space group $P6_3/m$) according to JCPDS card no. 09-0432, and exhibiting single-crystalline nature [10,11]. No obvious diffraction peaks from other impurities can be detected, indicating that the most of the impurities were removed effectively from the phosphogypsum waste through the proposed process. Application of the Scherrer equation to the (0 0 2) diffraction peak of the nHAp ($2\theta = 25.87°$) suggested a crystal size of 28 nm [25]. The diffraction peak of the (0 0 2) Miller plane family is chosen for calculation of the crystalline size, as it is isolated from other peaks. Also, this peak is relatively sharper than the other peaks, as shown in Fig. 2, corresponding to the crystal growth following the *c*-axis of the HAp structure [26,27].

The chemical composition of the raw PG and nHAp derived from PG evaluated by EDS analysis are presented in Table 1. According to this data the main components of the PG are $CaSO_4$ (expressed as CaO and SO_3), SiO_2, Al_2O_3, Fe_2O_3, MnO_2, MgO, K_2O and P_2O_5. Correspondingly, the major components of the nHAp derived from PG are CaO and P_2O_5, the molar ratio of Ca to P is about 1.66, approximating the stoichiometric proportion of that in $Ca_{10}(PO_4)_6(OH)_2$ molecule (≈1.67), indicates that HAp with high purity was prepared successfully through the proposed process using phosphogypsum as raw material. As shown in Table 1, the impurities were removed from the PG effectively, no SiO_2, Fe_2O_3 and MnO_2 were detected and the content of other impurities, such as SO_3, MgO, Al_2O_3 and K_2O, was considerably reduced. As the raw PG samples were treated by HCl solution, calcium sulphate, the main component of PG, dissolved in the acid solution according to the following reaction:

$$CaSO_4 + H^+ \rightarrow Ca^{2+} + HSO_4^- \quad (3)$$

The others acid-soluble oxide, such as Al_2O_3, Fe_2O_3, MnO_2, MgO and K_2O also dissolved in hydrochloric acid solution, while the SiO_2 and others acid-insoluble substance were removed by filtration. As the pH of the filtrate was adjusted to 9, most of the metal ions (e.g., Al^{3+}, Fe^{3+}, Mn^{2+} and Mg^{2+}) produced hydroxide precipitates and were separated off from the solution by filtration. The others impurities with good solubility in both of acid and alkaline solution, such as K^+, Na^+, SO_4^{2-} and Cl^- were removed by careful washing of the final product. The process described above guarantees the effective removal of the impurities from raw PG and the high purity of nHAp derived from PG.

The morphology of the nHAp derived from PG was examined by TEM. As shown in Fig. 3, the as-prepared nHAp particles show a short rod-like crystal structure with the particle size about 20 nm × 60 nm. The nanoparticles were observed to be easily dispersed in the ethanol solvent.

3.2. Effect of nHAp dosage on the removal of fluoride

Fig. 4 shows the effect of nHAp dosage on the removal of fluoride from aqueous solution. It can be seen that the nHAp derived from PG exhibited excellent removal efficiency for fluoride. As shown in Fig. 4, 1 g of nHAp can remove more than 99.3% of F^- from 100 mL of 50 mg F^-/L solution. For the fluoride solution with a relative lower concentration (10 mg F^-/L), a minimum adsorbent dosage of 0.3 g (i.e. 3 g/L) was enough to remove 99% of F^- ion. Meanwhile, it was found that increasing the adsorbent dosage increased the percent removal until the percent removal approached to nearly 100%. For example, as the increase in nHAp dosage from 1 to 5 g/L, the percent removal of F^- for 30 mg F^-/L solution increased rapidly from 42.0 to 96.6% due to the increment of the available surface area and adsorption sites [28]. With a further increase in nHAp dosage to 10 g/L, the percent removal increased to 99.7%. The results indicated that the nHAp derived from PG can be used as an efficient adsorbent for removal of fluoride from aqueous solution.

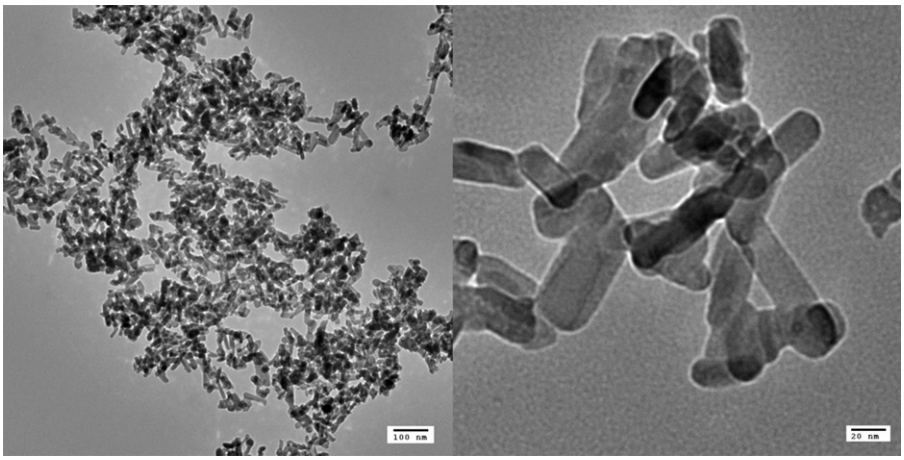

Fig. 3. TEM images of nHAp derived from PG prepared under microwave irradiation.

3.3. Effect of pH

The effect of pH on the adsorption of fluoride onto the nHAp derived from PG was studied in the pH range of 2–11, which was adjusted with HCl or NaOH in the beginning of the experiment and not controlled afterwards. As shown in Fig. 5, the adsorption capacity of the nHAp derived from PG for fluoride was highly dependent on proton concentration in the solution. It was clear that the adsorption capacity decreased sharply when the pH was lower than 6. The maximal adsorption capacity was 80 mg F^-/g (80% removal) at pH 2, and only 19.9 mg F^-/g at pH 6 (19.9% removal). As the pH increased further to 11, the adsorption capacities decreased slight to 14.9 mg F^-/g (14.9% removal). It is well known that the pH of the aqueous solution plays an important role, which controls the adsorption at the water adsorbent interface [15]. The computational study by means of molecular dynamics simulation elucidated that the apatite hydroxyl ions may not be directly protonated by aqueous protons due to that the embedding calcium triangles in HAp crystal structure prevent the interfacial water molecules from forming hydrogen bonds with the hydroxide ions in neutral medium [29]. But at low pH, acidic medium destroys the embedding calcium triangles structure, which induces the protonation at the surface of the HAp and thereby results in a larger number of active sites on the surface of HAp. The attractive forces between positively charged surface and negatively charged fluoride ions enhanced the adsorption of fluoride onto the surface of HAp. On the contrast, the surfaces of HAp are saturated with negative charge in alkaline medium, which hinder the diffusion of fluoride ions to HAp surface and a reasonable lower adsorption capacity was observed.

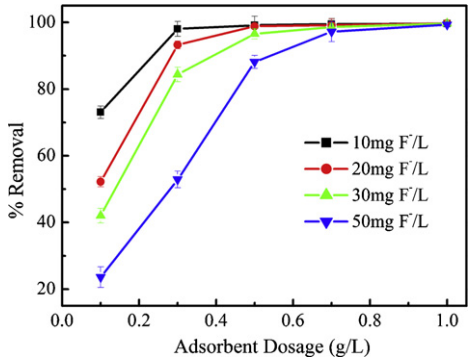

Fig. 4. Effect of nHAp dosage on percent removal of fluoride.

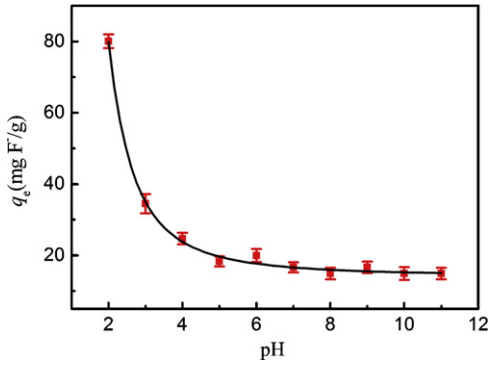

Fig. 5. Effect of pH on the adsorption of fluoride onto nHAp derived from PG.

3.4. Adsorption kinetics

Fig. 6 shows the kinetic adsorption behaviour of fluoride ions by nHAp derived from PG at neutral pH. The adsorption rate was fast in the beginning of the process, and then it decreased until equilibrium was reached. As shown in Fig. 6, the initial adsorption rate and adsorption amount at equilibrium increased with temperature, indicating that the higher temperature favours the adsorption of fluoride onto nHAp. Meanwhile, improving the adsorption capacity with temperature suggested that active centres on the surface available for adsorption increased with the temperature. This could also be attributed to the enhancing rate of intraparticle diffusion of solute since diffusion is an endothermic process [30].

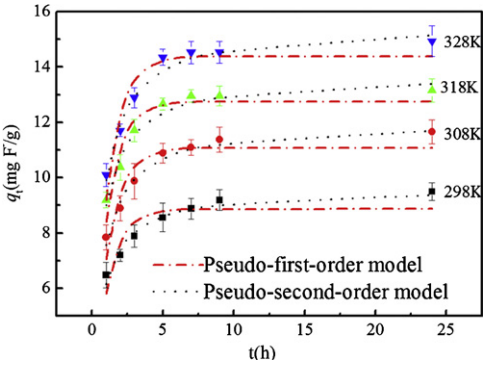

Fig. 6. Pseudo-first-order and pseudo-second-order kinetics for adsorption of fluoride onto nHAp derived from PG at different temperatures.

Table 2
Pseudo-first-order and second-order kinetics parameters of nHAp derived from PG.

T (K)	Pseudo-first-order kinetics				Pseudo-second-order kinetics			
	q_t (mg F$^-$/g)	k_1 (h^{-1})	R^2	ϕ	q_t (mg F$^-$/g)	k_2 (g/mg h)	R^2	ϕ
298	8.87	1.066	0.759	7.1	9.59	0.187	0.962	2.9
308	11.08	1.010	0.833	6.4	11.98	0.143	0.976	2.3
318	12.75	1.074	0.860	5.5	13.68	0.140	0.968	2.5
328	14.5	1.021	0.874	5.2	15.50	0.115	0.977	2.1

In order to investigate the controlling mechanism of adsorption process, the experimental data were modelled by the pseudo-first-order [31], and pseudo-second-order kinetics equations [32].

(1) Pseudo-first-order model

A pseudo-first-order model can be expressed in a non-linear form as

$$q_t = q_e(1 - e^{-k_1 t}) \tag{4}$$

where q_t is the adsorption amount of fluoride ions (mg F$^-$/g) at time t (min), q_e is the adsorption amount of fluoride at equilibrium (mg F$^-$/g), and k_1 is the equilibrium rate constant of pseudo-first-order adsorption (h^{-1}).

(2) Pseudo-second-order model

The adsorption kinetics may also be described by a pseudo-second-order kinetics model. The non-linear form of the model is

$$q_t = \frac{q_e^2 k_2 t}{1 + q_e k_2 t} \tag{5}$$

where k_2 is the pseudo-second-order rate constant of adsorption (g mg^{-1} h^{-1}).

Normalized standard deviation ϕ was used as the objective function to be minimized [33]:

$$\phi = 100\sqrt{\frac{(q_{exp} - q_{cal}/q_{exp})^2}{N_i - 1}} \tag{6}$$

where q_{exp} (mg F$^-$/g) is the experimental fluoride uptake, q_{cal} (mg F$^-$/g) is the calculated amount of fluoride ion adsorbed and N_i is the number of data points.

The non-linear fitted curves of the models along with the experimental data are illustrated in Fig. 6. The corresponding parameters and normalized standard deviation are included in Table 2. It is found that the fitting data to the pseudo-second-order model gave the higher R^2 values of coefficients and lower ϕ values of normalized standard deviation than those for the pseudo-first-order kinetics model at all test temperatures, viz., 298, 308, 318 and 328 K. The results illuminated that the pseudo-first-second model fitted better the experimental data than the pseudo-second-order model.

As the above kinetic models were not able to identify the diffusion mechanism, thus intraparticle diffusion model based on the theory proposed by Weber and Morris [34] was tested. According to this theory:

$$q_t = k_{di} t^{1/2} + c_i \tag{7}$$

where k_{di} is an intraparticle diffusion rate parameter (mg/g h$^{1/2}$). c_i is the intercept of stage i, which gives an idea about the thickness of boundary layer.

Fig. 7 shows a plot of the Weber and Morris intraparticle diffusion model for the adsorption of fluoride onto nHAp derived from PG. It can be seen that these plots are multi linear curves with three distinct regions due to the varying extent of adsorption in the initial, middle and final stages of the experiment, which indicates that three or more steps occurred in the adsorption of fluoride ions. The initial rapid sharper portion attributes to the boundary layer diffusion of solute molecules corresponding to instantaneous adsorption or external surface adsorption was completed within the first 1 h for all test temperatures. After the external surface loading was completed, the intraparticle diffusion takes place. The second portion describes the gradual adsorption stage, where the transportation of F$^-$ within nHAp particles is rate limiting. The third portion is attributed to the final equilibrium stage where intraparticle diffusion starts to slow down due to extremely low adsorbate concentrations in the solution [35,36]. It is well known that if intraparticle diffusion occurs, then q_t vs $t^{1/2}$ will be linear and if the plot passes through the origin, then the rate limiting process is only due to the intraparticle diffusion. Otherwise, some other mechanism along with intraparticle diffusion is also involved [35]. As can be seen from Fig. 7, the linear lines of the second and third stages did not pass through the origin, indicating that intraparticle diffusion was not the only rate limiting mechanism in this adsorption process.

3.5. Adsorption isotherms

Equilibrium relationships between adsorbent and adsorbate are described by adsorption isotherms. The adsorption isotherm is important from both a theoretical and a practical point of view, isotherm data should accurately fit to different isotherm models to find a suitable model that can be used for the design of adsorption process. The experimental data obtained in the present work were tested by the Langmuir [37], Freundlich [38], Langmuir–Freundlich [39], and Tempkin models [40]. The non-linear form of Langmuir isotherm is represented by the following equation:

$$q_e = \frac{q_m K_a c_e}{1 + K_a c_e} \tag{8}$$

where c_e (mg F$^-$/L) is the equilibrium concentration of the fluoride, q_m (mg F$^-$/g) is the maximum adsorption at monolayer coverage and K_a (L/mg) is the constant related to the extent of adsorption, respectively.

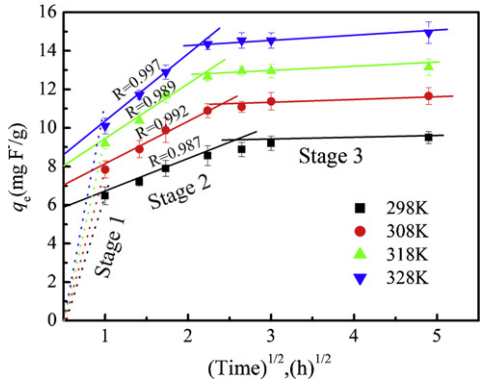

Fig. 7. Plot of intraparticle diffusion model for adsorption of fluoride onto nHAp derived from PG at different temperatures.

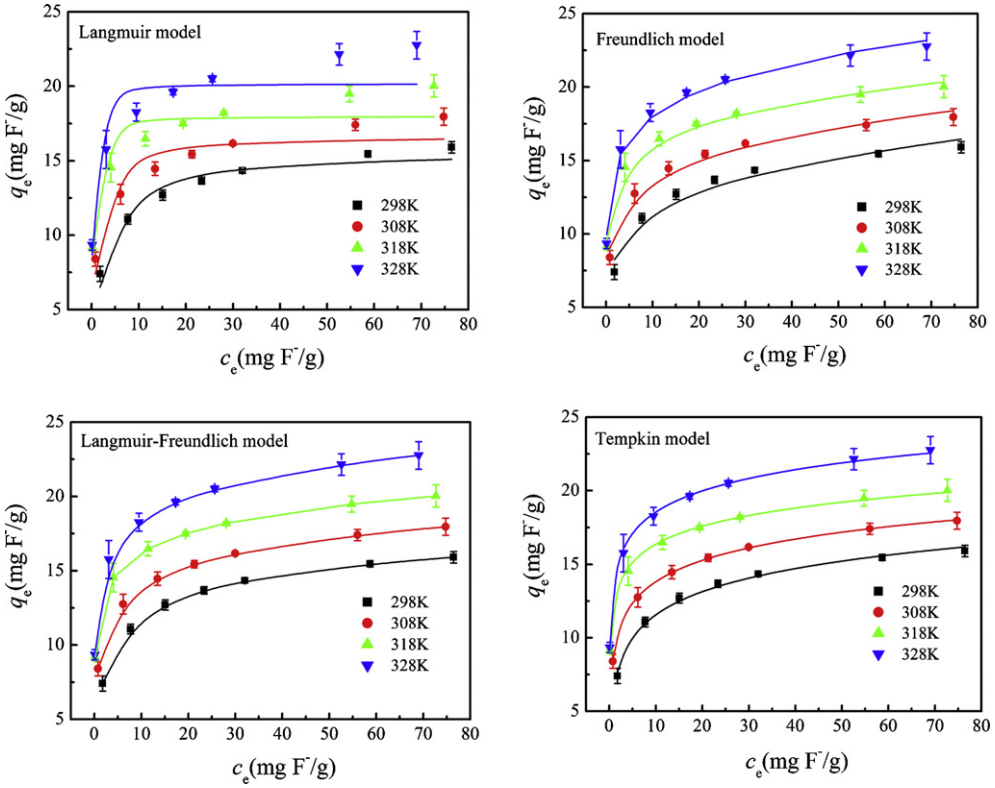

Fig. 8. Adsorption isotherms of fluoride at various temperatures.

The non-linear form of Freundlich isotherm is written as follow:

$$q_e = K_F c_e^{1/n_F} \tag{9}$$

where K_F and n_F are Freundlich constants with n_F giving an indication of how favourable the adsorption process and K_F (mg/g) related to the bonding energy.

The Langmuir–Freundlich model is expressed as:

$$q_e = q_m \frac{bc_e^{1/n}}{1 + bc_e^{1/n}} \tag{10}$$

where q_m (mg F^-/L) is the monolayer-adsorption capacity, b (L/mg) and n are the constants in the Langmuir–Freundlich equation.

The non-linear form of Tempkin isotherm is given by:

$$q_e = B_T \ln A + B_T \ln C_e \tag{11}$$

where A (L/mg) and B_T (J/mol) are the Tempkin constants.

Different adsorption isotherms obtained by using non-linear regression at various temperatures are illustrated in Fig. 8. The parameters of these models and normalized standard deviation are given in Table 3. As can be seen from Fig. 8 and Table 3, Freundlich, Langmuir–Freundlich, and Tempkin models fit the experimental data well, the correlation coefficient R^2 for these models are all higher than 0.96 while the correlation coefficient R^2 for Langmuir model is just higher than 0.77. The correlation coefficient and normalized standard deviations obtained during data fitting suggest that Freundlich, Langmuir–Freundlich, and Tempkin models

Table 3
Isotherm parameters obtained from the non-linear fitting of various models to the adsorption data of fluoride onto nHAp derived from PG.

Model	Parameters	298 K	308 K	318 K	328 K
Langmuir	q_m (mg F^-/L)	15.589	16.647	17.984	20.169
	K_a (L/mg)	0.402	1.060	5.859	7.130
	R^2	0.937	0.850	0.801	0.778
	ϕ	6.7	9.0	10.1	11.9
Freundlich	K_F (L/mg)	7.441	9.428	12.016	13.326
	n_F	5.473	6.463	8.143	9.652
	R^2	0.963	0.979	0.993	0.991
	ϕ	5.4	3.6	2.3	3.0
Langmuir–Freundlich	q_m (mg F^-/L)	19.742	26.108	36.914	40.818
	b (L/mg)	0.447	0.521	0.585	0.618
	n	1.950	2.992	4.472	4.791
	R^2	0.997	0.995	0.999	0.998
	ϕ	1.4	1.7	0.3	1.2
Tempkin	A (L/mg)	16.547	75.278	1010.690	761.468
	B_T (J/mol)	2.264	2.085	1.774	2.075
	R^2	0.991	0.992	0.997	0.995
	ϕ	2.1	1.7	1.0	1.5

Table 4
Thermodynamic parameters for adsorption of fluoride onto nHAp derived from PG.

T (K)	ΔG° (kJ/mol)	ΔH° (kJ/mol)	ΔS° (J/mol K)
298	0.88	27.39	88.96
308	−0.01		
318	−0.90		
328	−1.79		

describe the present adsorption system sufficiently well and Langmuir model do not match the data satisfactorily. A comparison of different isotherm models reveals that Langmuir–Freundlich model fits the experimental data best, suggesting that the nHAp derived from waste PG may be heterogeneous with a different energy distribution [41]. Tempkin and Freundlich isotherms were all better than Langmuir isotherm, implying that the adsorption process involved multimolecular layers of coverage and the effects of some indirect adsorbate/adsorbate interactions might occur in adsoprion of fluoride ions onto nHAp derived from waste PG [38,40,42].

3.6. Thermodynamic parameters

In order to understand the effect of temperature on the adsorption process, thermodynamic parameters associated with the adsorption viz., standard free energy change (ΔG°), standard enthalpy change (ΔH°) and standard entropy change (ΔS°) were calculated and presented in Table 4.

The standard enthalpy change (ΔH°) and standard entropy change (ΔS°) were calculated by using the equation:

$$\ln K_o = \frac{\Delta S^\circ}{R} - \frac{\Delta H^\circ}{RT} \quad (12)$$

where ΔH° is the standard enthalpy change (kJ/mol), ΔS° is the standard entropy change (J/mol K), T is the temperature in Kelvin, R is the universal gas constant (8.314 J/mol K) and K_o is the adsorption equilibrium constant. The adsorption equilibrium constant K_o for the adsorption reaction was determined from the slope of the plot of $\ln(q_e/c_e)$ vs c_e at different temperatures and extrapolating to zero c_e according to method suggested by Khan and Singh [15,43]. The values of ΔH° and ΔS° can be obtained from the slope and intercept of a plot of $\ln K_o$ against $1/T$.

The free energy of adsorption process is given by the equation:

$$\Delta G^\circ = \Delta H^\circ - T\Delta S^\circ \quad (13)$$

where ΔG° is the standard free energy change (kJ/mol).

The value of ΔG° indicated the adsorption process was non-spontaneous at lower temperature and spontaneous at higher temperature, the transition temperature was about 308 K. Meanwhile, the small value of ΔG° implied the adsorptive forces were strong enough to overcome the potential barrier [44]. The positive value of ΔH° suggested the endothermic nature of adsorption, which may be also predicted from the increase in value of fluoride uptake of the nHAp derived from PG with the rise in temperature. The positive value of ΔS° suggested an increase in randomness at the solid/solution interface during the adsorption process and a good affinity of fluoride with nHAp derived from PG [45].

3.7. Desorption

Desorption study gives an idea about the nature of adsorption. The result of the studies indicated that the desorption of the adsorbed fluoride in 100 mL of neutral distilled water, 0.001 N HCl and 0.001 N NaOH resulted about 0.83%, 3.12% and 21.86% for initial concentration of 50 mg F^-/L, respectively. The desorption studies showed higher desorption in alkali medium than in acidic and neutral medium. These results of more desorption under extremely high pH are consistent with the study of the effect of pH on the adsorption capacity and suggests that fluoride ions may be replaced by hydroxyl anions in alkali medium. Meanwhile, it is evident from the low desorption values, once fluoride are adsorbed over the surface of nHAp derived from PG, it is very difficult to regenerate.This probably reduces its relevance for fluoride adsorption. But due to its extremely high removal capacity (99%), it can be used in many places where water can be made completely free from fluoride.

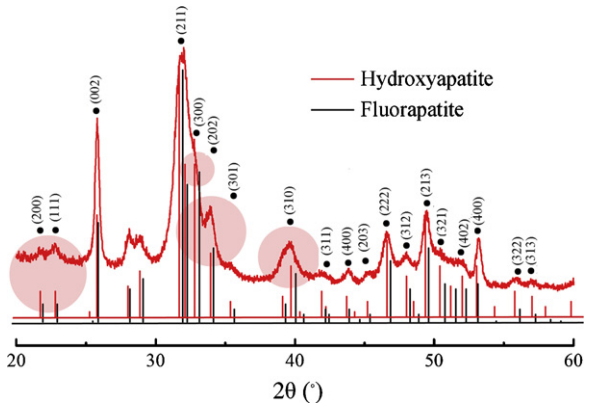

Fig. 9. XRD pattern of the nHAp derived from PG after adsorption.

3.8. Adsorption mechanism

The mechanism of fluoride adsorption onto nHAp particles had been reported in some literatures [15,46,47]. In general, both physical adsorption originating from electrostatic interaction and chemical adsorption from ion exchange were proposed as the main driving force for fluoride uptake onto HAp surfaces [15,16,46–48]. The ion exchange reaction between HAp and fluoride follows the equations:

$$Ca_{10}(PO_4)_6(OH)_2 + F^- \rightarrow Ca_{10}(PO_4)_6(F, OH) + OH^- \quad (14)$$

It can be seen that fluorapatite or hydroxyfluorapatite is the resulted product of ion exchange reaction. To investigate whether this process participated in the adsorption of fluoride onto nHAp derived from PG, XRD pattern of the nHAp which had equilibrated at 100 mL of 100 mg F^-/L solution for 24 h at neutral pH was inspected and recorded in Fig. 9. As shown in Fig. 9, all diffraction peaks were assigned to HAp (re. PDF#09-0432), indicated that HAp still was the main phase composition after adsoprtion of fluoride. Meanwhile, according to Eq. (14), adsorption process of fluoride ions releases OH^-, thus the solution pH after reaction changed. So, the change of solution pH was monitored continuously and recorded in Fig. 10. As shown in Fig. 10, the pH of the solution increased with the

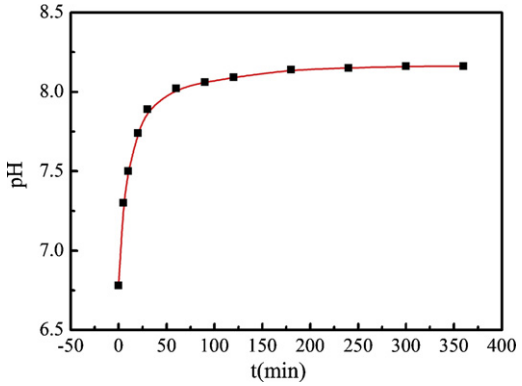

Fig. 10. The change of solution pH in the adsorption of fluoride onto nHAp derived from PG (0.2 g nHAp, 100 mL of 50 mg F^-/L fluoride solution, 298 K).

contact time and reached the equilibrium after 120 min. It can be seen from the adsorption kinetics study that the adsorption equilibrium was reached after 5 h, which was much more than the equilibrium time of pH. These results clarified that the ion exchange reaction between nHAp derived from PG and fluoride only occurred at the initial stage of adsorption and was not the major driving force for fluoride uptake onto nHAp derived from PG. Molecular dynamics simulations of the incorporation of fluoride into hydroxyapatite proved that fluoride ions are easily incorporated from solution into the surfaces of hydroxyapatite, but they do not segregate into the bulk crystal beyond approximately10 Å [49]. So, it was reasonable to conclude that ion exchange between HAp and fluoride occurred only on the surfaces of the hydroxyapatite crystal. Meanwhile, the nHAp derived from PG exhibited excellent adsoption capacity for fluoride, the maximum adsorption capacities calculated from Langmuir–Freundlich model were 19.742, 26.108, 36.914 and 40.818 mg F^-/g for 298, 308, 318 and 328 K, respectively, which were more larger than that of nHAp particles synthesized directly [15,46,47] and even larger than that of most normal adsorbent for fluoride, such as activated carbon [44], montmorillonite [50], porous granular ceramic [51], granular red mud [52] and chitosan derivatives and composites [53]. As shown in Table 1, most of the impurities were separated from phosphogypsum, but there were still a lot of metal elements, e.g., Al^{3+}, incorporated into as-prepared nHAp crystal, which generated some defects in nHAp crystal, and destroyed the charges balance at nHAp surfaces. The distribution of these metal elements within nHAp crystal was not uniform, resulting the charge distributions of nHAp surface were heterogeneous, which provided some additional adsorption sites for fluoride through electrostatic interaction. So, in view of the extraordinary adsorption capacity of nHAp derived from PG, it was reasonable to propose that electrostatic interaction and hydrogen bond were the main driving force for fluoride uptake onto nHAp surfaces derived from PG.

4. Conclusion

The hydroxyapatite nanoparticles derived from PG exhibited a hexagonal structure with the particle size about 20 nm × 60 nm and high purity. The nHAp derived from PG show a good efficiency in fluoride removal from aqueous solution. The maximum adsorption capacities calculated from Langmuir–Freundlich model are 19.742, 26.108, 36.914 and 40.818 mg F^-/g for 298, 308, 318 and 328 K at neutral pH, respectively, and bigger capacities for fluoride removal were observed at lower pH, indicating that the adsorbent has promising potential utility in practical application. Kinetic study results indicated that the adsorption process followed a pseudo-second-order kinetic model and the adsorption isotherm could be well defined by Langmuir–Freundlich equation. Electrostatic interaction and hydrogen bond are proposed as the main driving force for fluoride uptake onto nHAp surfaces derived from waste phosphogypsum.

Acknowledgements

This work was supported by grant no. 1112RJZA024 of the Natural Science Foundation of Gansu and the Hongliu Young Teacher Cultivate Project of Lanzhou University of Technology.

References

[1] H. Tayibi, M. Choura, F.A. López, F.J. Alguacil, A. López-Delgado, Environmental impact and management of phosphogypsum, J. Environ. Manage. 90 (2009) 2377–2386.
[2] S. Çoruh, O.N. Ergun, Use of fly ash, phosphogypsum and red mud as a liner material for the disposal of hazardous zinc leach residue waste, J. Hazard. Mater. 173 (2010) 468–473.
[3] R. Pérez-López, J. Castillo, A.M. Sarmiento, J.M. Nieto, Assessment of phosphogypsum impact on the salt-marshes of the Tinto river (SW Spain): role of natural attenuation processes, Mar. Pollut. Bull. 62 (2011) 2787–2796.
[4] J. Yang, W. Liu, L. Zhang, B. Xiao, Preparation of load-bearing building materials from autoclaved phosphogypsum, Constr. Build. Mater. 23 (2009) 687–693.
[5] N. Değirmenci, Utilization of phosphogypsum as raw and calcined material in manufacturing of building products, Constr. Build. Mater. 22 (2008) 1857–1862.
[6] C. Papastefanou, S. Stoulos, A. Ioannidou, M. Manolopoulou, The application of phosphogypsum in agriculture and the radiological impact, J. Environ. Radioact. 89 (2006) 188–198.
[7] N. Degirmenci, A. Okucu, A. Turabi, Application of phosphogypsum in soil stabilization, Build. Environ. 42 (2007) 3393–3398.
[8] J. Zhou, H. Gao, Z. Shu, Y. Wang, C. Yan, Utilization of waste phosphogypsum to prepare non-fired bricks by a novel hydration–recrystallization process, Constr. Build. Mater. 34 (2012) 114–119.
[9] M. Betsiou, G. Bantsis, I. Zoi, C. Sikalidis, Adsorption and release of gemcitabine hydrochloride and oxaliplatin by hydroxyapatite, Ceram. Int. 38 (2012) 2719–2724.
[10] X. Guo, W. Wang, G. Wu, J. Zhang, C. Mao, Y. Deng, H. Xia, Controlled synthesis of hydroxyapatite crystals templated by novel surfactants and their enhanced bioactivity, New J. Chem. 35 (2011) 663.
[11] D.K. Lee, J.Y. Park, M.R. Kim, D.J. Jang, Facile hydrothermal fabrication of hollow hexagonal hydroxyapatite prisms, Cryst. Eng.Comm. 13 (2011) 5455–5459.
[12] V.D.B.C. Dasireddy, S. Singh, H.B. Friedrich, Oxidative dehydrogenation of n-octane using vanadium pentoxide-supported hydroxyapatite catalysts, Appl. Catal. A: Gen. 421–422 (2012) 58–69.
[13] S. Wang, Y. Lei, Y. Zhang, J. Tang, G. Shen, R. Yu, Hydroxyapatite nanoarray-based cyanide biosensor, Anal. Biochem. 398 (2010) 191–197.
[14] I. Smičiklas, S. Dimović, I. Plećaš, M. Mitrić, Removal of Co^{2+} from aqueous solutions by hydroxyapatite, Water Res. 40 (2006) 2267–2274.
[15] C.S. Sundaram, N. Viswanathan, S. Meenakshi, Defluoridation chemistry of synthetic hydroxyapatite at nano scale: equilibrium and kinetic studies, J. Hazard. Mater. 155 (2008) 206–215.
[16] M. Jiménez-Reyes, M. Solache-Ríos, Sorption behavior of fluoride ions from aqueous solutions by hydroxyapatite, J. Hazard. Mater. 180 (2010) 297–302.
[17] S.H. Tan, X.G. Chen, Y. Ye, J. Sun, L.Q. Dai, Q. Ding, Hydrothermal removal of Sr^{2+} in aqueous solution via formation of Sr-substituted hydroxyapatite, J. Hazard. Mater. 179 (2010) 559–563.
[18] I. Mobasherpour, E. Salahi, M. Pazouki, Removal of divalent cadmium cations by means of synthetic nano crystallite hydroxyapatite, Desalination 266 (2011) 142–148.
[19] H. Zhang, M. Liu, H. Fan, X. Zhang, An efficient method to synthesize carbonated nano hydroxyapatite assisted by poly(ethylene glycol), Mater. Lett. 75 (2012) 26–28.
[20] K.P. Sanosh, M.C. Chu, A. Balakrishnan, Y.J. Lee, T.N. Kim, S.J. Cho, Synthesis of nano hydroxyapatite powder that simulate teeth particle morphology and composition, Curr. Appl. Phys. 9 (2009) 1459–1462.
[21] A.A. Chaudhry, S. Haque, S. Kellici, P. Boldrin, I. Rehman, F.A. Khalid, J.A. Darr, Instant nano-hydroxyapatite: a continuous and rapid hydrothermal synthesis, Chem. Commun. 21 (2006) 2286–2288.
[22] J. Liu, K. Li, H. Wang, M. Zhu, H. Yan, Rapid formation of hydroxyapatite nanostructures by microwave irradiation, Chem. Phys. Lett. 396 (2004) 429–432.
[23] Z. Yang, Y. Jiang, Y. Wang, L. Ma, F. Li, Preparation and thermal stability analysis of hydroxyapatite derived from the precipitation process and microwave irradiation method, Mater. Lett. 58 (2004) 3586–3590.
[24] S.J. Kalita, S. Verma, Nanocrystalline hydroxyapatite bioceramic using microwave radiation: synthesis and characterization, Mater. Sci. Eng. C 30 (2010) 295–303.
[25] C.W. Chen, C.S. Oakes, K. Byrappa, R.E. Riman, K. Brown, K.S. TenHuisenb, V.F. Janas, Synthesis characterization, and dispersion properties of hydroxyapatite prepared by mechanochemical–hydrothermal methods, J. Mater. Chem. 14 (2004) 2425–2432.
[26] A. Siddharthan, S. Seshadri, T. Kumar, Influence of microwave power on nanosized hydroxyapatite particles, Scr. Mater. 55 (2006) 175–178.
[27] E. Bouyer, F. Gitzhofer, M.I. Boulos, Morphological study of hydroxyapatite nanocrystal suspension, J. Mater. Sci. Mater. Med. 1 (2000) 523–531.
[28] W. Wei, R. Sun, J. Cui, Z. Wei, Removal of nitrobenzene from aqueous solution by adsorption on nanocrystalline hydroxyapatite, Desalination 263 (2010) 89–96.
[29] D. Zahn, O. Hochrein, Computational study of interfaces between hydroxyapatite and water, Phys. Chem. Chem. Phys. 5 (2003) 4004–4007.
[30] M. Zabihi, A. Ahmadpour, A.H. Asl, Removal of mercury from water by carbonaceous sorbents derived from walnut shell, J. Hazard. Mater. 167 (2009) 230–236.
[31] S. Lagergren, Zur theorie der sogenannten adsorption gelöster stoffe, Kungliga Svenska Vetenskapsakademiens, Handlingar 24 (1898) 1–39.
[32] Y.S. Ho, G. McKay, Sorption of dye from aqueous solution by peat, Chem. Eng. J. 70 (1998) 115–124.
[33] A. Eskandarpour, M.S. Onyango, A. Ochieng, S. Asai, Removal of fluoride ions from aqueous solution at low pH using schwertmannite, J. Hazard. Mater. 152 (2008) 571–579.
[34] W.J. Weber, J.C. Morris, Kinetics of adsorption on carbon from solution, J. Sanit. Eng. Div. Am. Soc. Civ. Eng. 89 (1963) 31–59.
[35] I.A.W. Tan, A.L. Ahmad, B.H. Hameed, Adsorption isotherms kinetics, thermodynamics and desorption studies of 2,4,6-trichlorophenol on oil palm empty fruit bunch-based activated carbon, J. Hazard. Mater. 164 (2009) 473–482.

[36] A.S.A. Lzaydien, Adsorption of methylene blue from aqueous solution onto a low-cost natural Jordanian tripoli, Am. J. Environ. Sci. 5 (2009) 197–208.
[37] Langmuir, The adsorption of gases on plane surfaces of glass mica, and platinum, J. Am. Chem. Soc. 40 (1918) 1361–1402.
[38] H. Freundlich, Adsorption in solution, Z. Phys. Chem. 57 (1906) 384–470.
[39] R. Sips, On the structure of a catalyst surface, J. Chem. Phys. 16 (1948) 490–501.
[40] M.J. Tempkin, V. Pyzhev, Kinetics of ammonia synthesis on promoted iron catalysts, Acta Physiochim. URSS 12 (1940) 217–222.
[41] A. Derylo-Marczewska, M. Jaroniec, D. Gelbin, A. Seidel, Heterogeneity effects in single-solute adsorption from dilute solutions on solids, Chem. Scr. 24 (1984) 239–244.
[42] K. Li, Z. Zheng, X. Huang, G. Zhao, J. Feng, J. Zhang, Equilibrium, kinetic and thermodynamic studies on the adsorption of 2-nitroaniline onto activated carbon prepared from cotton stalk fibre, J. Hazard. Mater. 166 (2009) 213–220.
[43] A.A. Khan, R.P. Singh, Adsorption thermodynamics of carbofuran on Sn (IV) arsenosilicate in H^+, Na^+ and Ca^{2+} forms, Colloids Surf. 24 (1987) 33–42.
[44] A. Daifullah, S. Yakout, S. Elreefy, Adsorption of fluoride in aqueous solutions using $KMnO_4^-$ modified activated carbon derived from steam pyrolysis of rice straw, J. Hazard. Mater. 147 (2007) 633–643.
[45] B. Kemer, D. Ozdes, A. Gundogdu, V.N. Bulut, C. Duran, M. Soylak, Removal of fluoride ions from aqueous solution by waste mud, J. Hazard. Mater. 168 (2009) 888–894.
[46] Y. Wang, N. Chen, W. Wei, J. Cui, Z. Wei, Enhanced adsorption of fluoride from aqueous solution onto nanosized hydroxyapatite by low-molecular-weight organic acids, Desalination 276 (2011) 161–168.
[47] C. Sairam Sundaram, N. Viswanathan, S. Meenakshi, Fluoride sorption by nano-hydroxyapatite/chitin composite, J. Hazard. Mater. 172 (2009) 147–151.
[48] W. Liang, L. Zhan, L. Piao, C. Rűssel, Fluoride removal performance of glass derived hydroxyapatite, Mater. Res. Bull. 46 (2011) 205–209.
[49] N.H.d. Leeuw, A computer modelling study of the uptake and segregation of fluoride ions at the hydrated hydroxyapatite (0 0 0 1) surface introducing a $Ca_{10}(PO_4)_6(OH)_2$ potential model, Phys. Chem. Chem. Phys. 6 (2004) 1860–1866.
[50] A. Tor, Removal of fluoride from an aqueous solution by using montmorillonite, Desalination 201 (2006) 267–276.
[51] N. Chen, Z. Zhang, C. Feng, D. Zhu, Y. Yang, N. Sugiura, Preparation and characterization of porous granular ceramic containing dispersed aluminum and iron oxides as adsorbents for fluoride removal from aqueous solution, J. Hazard. Mater. 186 (2011) 863–868.
[52] A. Tor, N. Danaoglu, G. Arslan, Y. Cengeloglu, Removal of fluoride from water by using granular red mud: batch and column studies, J. Hazard. Mater. 164 (2009) 271–278.
[53] P. Miretzky, A.F. Cirelli, Fluoride removal from water by chitosan derivatives and composites: a review, J. Fluorine Chem. 132 (2011) 231–240.